Evaluation of Strength Recovery and Analysis of Damage Progression of Notched Unidirectional Carbon/Epoxy Composites Encompassing Self-Healing of Interfacial Debonding

Kazuaki Sanada[1,*], Yuta Mizuno[1], Yasuhide Shindo[2]

[1] Department of Mechanical Systems Engineering, Toyama Prefectural University, Toyama 939-0398, Japan
[2] Department of Materials Processing, Graduate School of Engineering, Tohoku University, Sendai 980-8597, Japan
* Corresponding author: sanada@pu-toyama.ac.jp

Abstract This study examines the interfacial debonding behavior of self-healing fiber reinforced polymers (FRPs) and the performance of repair of interfacial debonding. Self-healing is accomplished by incorporating a microencapsulated healing agent and a catalyst within a coating layer on the surface of the fiber strand. Single edge notched tensile (SENT) specimens of unidirectional FRPs with coated fiber strands were prepared and tested. The healing efficiency was evaluated by the critical fracture loads of virgin and healed specimens. To investigate the release of the healing agent from microcapsules during interfacial debonding, an ultra-violet (UV) fluorescent dye was added to the healing agent and post-fracture specimens were examined by an optical microscope under UV light. In addition to conducting experiments, finite element analyses were performed using a three-dimensional model to predict the damage progression in SENT specimens.

Keywords Interface mechanics, Composite materials, Notched tensile strength, Damage progression, Self-healing

1. Introduction

Interfacial debonding can cause a reduction in strength and stiffness of fiber-reinforced polymers (FRPs) and is extremely difficult to detect and repair by conventional methods. Thus, self-healing has the potential to mitigate the interfacial debonding. Although many studies have addressed the self-healing of internal damage in FRPs, there are few reports on the self-healing of interfacial debonding. Sanada et al. [1] proposed a methodology for self-healing of interfacial debonding in unidirectional FRPs by using fiber strands coated with the self-healing polymer developed by White et al. [2] and conducted transverse tensile tests to assess the self-healing efficiency. Also, Sanada et al. [3] investigated the effect of microstructure on the efficiency of transverse tensile strength recovery of self-healing FRPs. The maximum healing efficiency achieved with these specimens was about 20% and the low healing efficiency achieved was due to complete rupture of virgin specimens. Blaiszik et al. [4] performed a microbond test using a single fiber coated with DCPD-filled microcapsules and Grubbs catalyst, and assessed the recovery of interfacial shear strength.

The aim of this study is to investigate the interfacial debonding behavior of self-healing FRPs and to assess the performance of self-healing system for interfacial debonding. Tensile tests were carried out with single edge notched tensile (SENT) specimens of unidirectional FRPs containing fiber strands coated with DCPD-filled microcapsules and Grubbs catalyst, and healing efficiency was calculated using the critical fracture loads of virgin and healed specimens. Fluorescent labeling of damage in post-fracture specimens was performed to study the release of DCPD from microcapsules during interfacial debonding. Additionally, finite element analyses were employed to study the effect of specimen thickness and coating properties on the damage progression in SENT specimens.

2. Experimental procedures
2.1. Materials and specimen preparation

Self-healing FRP and reference FRP plates made of unidirectional carbon fiber-reinforced polymer were prepared. For self-healing FRP plates as shown in Fig. 1, Torayca T300B (Toray Industries, Inc.) carbon fiber strands were coated by manually dipping them into the Epikote 828 (Japan Epoxy Resins Co. Ltd)/Ancamine K54 (Air Products and Chemicals, Inc.) epoxy mixture containing 30wt% microcapsules and 2.5wt% Grubbs catalyst (Sigma-Aldrich Co.). Healing is triggered by crack propagation (interfacial debonding) through the microcapsules, which then release the healing agent into the crack plane. Subsequent exposure of the healing agent to the catalyst initiates polymerization and bonding of the crack faces. The number of filaments in the fiber strand was 6000. The healing agent used in this study was dicyclopentadiene (DCPD) monomer. DCPD was microencapsulated using the previously described procedure [1]. The microcapsules with mean diameter of around 300 μm were used. To aid inspection for the release of the healing agent from broken microcapsules, the microcapsules were also made from DCPD mixed with a UV fluorescent dye (Blenny Giken Ltd.). After coating, the coated fiber strands were held straight and cured for 24h at room temperature in order to obtain proper hardness. For reference FRP plates, coated carbon fiber strands without Grubbs catalyst were prepared using similar procedures.

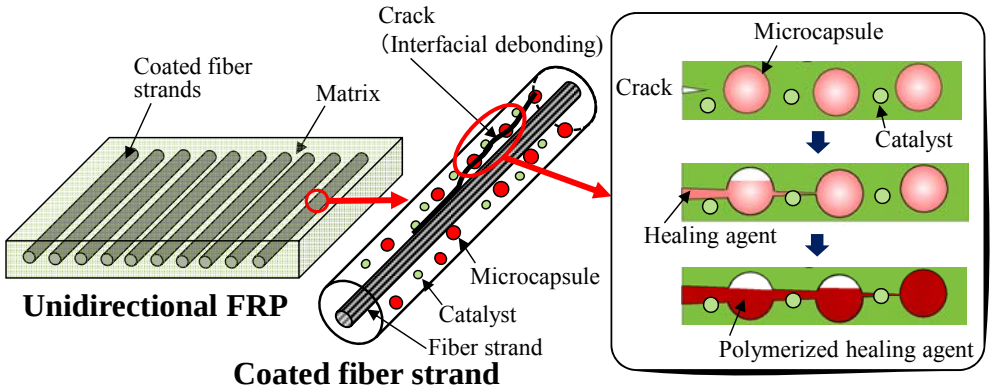

Figure 1 Self-healing system of interfacial debonding in unidirectional FRP

The semi-cured fiber strands were placed in a mold and impregnated with the Epikote 828/diethylenetriamine. The coated fiber strands were aligned parallel to the long direction. The mold was then closed and the samples were molded into the plate for 24h at room temperature, followed by 24h at 40°C .

Once the plates were cured, they were machined using a water cooled diamond saw to produce SENT specimens as shown in Fig. 2. The SENT specimens had a nominal width W of 20mm, a nominal thickness t of 2 or 3mm, a gage length L of 40mm and an overall length of 70mm. A notch was cut using a diamond wafering saw and a sharp pre-crack was created by gently tapping a razor blade into the notch in the specimens. All specimens had an initial notch length to specimen width ratio a_0/W of approximately 0.25. Aluminum alloy gripping tabs (approximately 1mm thickness) were mounted to the specimens to prevent crushing due to the serrated rip faces. The specimens with t =2 and 3mm contained a fiber volume fraction of about 3.4 and 5.1%, respectively.

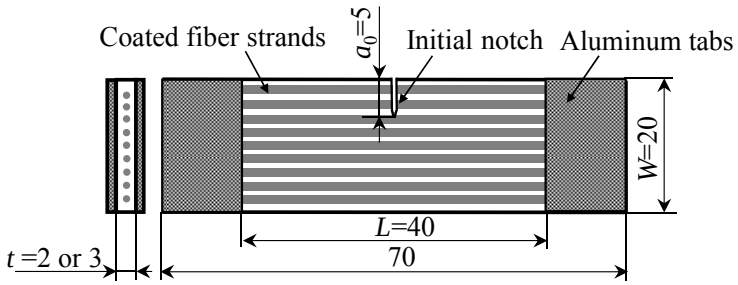

Figure 2 Specimen geometry (dimensions in mm)

2.2. Testing methods

The SENT specimens were tested using a tensile test machine in the displacement control at rate of 0.5mm/min. Load and crosshead displacement were recorded throughout the test. The self-healing FRP specimens were loaded until large load drops occurred, indicating damage progression. Before the specimens fractured completely, the specimens were unloaded and removed from the tensile test machine. Then, the specimens were clamped in a vise and allowed to heal for 10 days at room temperature. After healing, the specimens were tested again. For the reference FRP specimens, the specimens were immediately unloaded and reloaded to fracture after virgin tests, and the critical fracture load of the damaged specimen was evaluated. Healing efficiency η was defined as the ability of a healed specimen to recover critical fracture load

$$\eta = \frac{P_c^{\text{healed}} - P^{\text{residual}}}{P_c^{\text{virgin}} - P^{\text{residual}}} \tag{1}$$

where P_c^{virgin} is the critical fracture load of the virgin specimen, P_c^{healed} is the critical fracture load of the healed specimen and P^{residual} is the load value that was established at the end of the virgin test. To investigate the microstructure and damage behavior of the specimens, optical microscope observations were also performed.

2.3. Finite element analysis

The 3D finite element model was developed using ANSYS finite element code. A schematic diagram of the SENT specimen model is shown in Fig. 3. In this figure, R and h denote the radius of the fiber strand and the thickness of the coating layer, respectively. The geometric parameters of coated fiber strands as measured in the optical microscope were used. A rectangular Cartesian coordinate system (x_1, x_2, x_3) is used and x_1, x_2 and x_3 axes are assumed to lie along the longitudinal direction (fiber direction), transverse direction and thickness direction, respectively. Due to symmetry in both geometry and loading configurations, only one-quarter of the SENT specimens were modeled. Let the displacement and stress components be denoted by u_i^δ and σ_{ij}^δ $(i, j = 1,2,3, \delta = f, m, c)$, respectively. The subscripts 1, 2 and 3 are related to the three axes of the coordinate system and the superscripts f, m and c indicate the fiber strand, matrix and coating layer, respectively. The boundary conditions can be written as

$$\sigma_{11}^\delta(0, x_2, x_3) = 0 \quad (0 \le x_2 < a_0, 0 \le x_3 \le t/2) \tag{2}$$

$$u_1^\delta(0, x_2, x_3) = 0 \quad (a_0 \le x_2 \le W, 0 \le x_3 \le t/2) \tag{3}$$

$$\sigma_{12}^\delta(0, x_2, x_3) = 0 \quad (0 \le x_2 \le W, 0 \le x_3 \le t/2) \tag{4}$$

$$\sigma_{13}^{\delta}(0, x_2, x_3) = 0 \quad (0 \le x_2 \le W, 0 \le x_3 \le t/2) \tag{5}$$

$$u_1^{\delta}(L/2, x_2, x_3) = u_0 \quad (0 \le x_2 \le W, 0 \le x_3 \le t/2) \tag{6}$$

$$\sigma_{12}^{\delta}(L/2, x_2, x_3) = 0 \quad (0 \le x_2 \le W, 0 \le x_3 \le t/2) \tag{7}$$

$$\sigma_{13}^{\delta}(L/2, x_2, x_3) = 0 \quad (0 \le x_2 \le W, 0 \le x_3 \le t/2) \tag{8}$$

$$u_3^{\delta}(x_1, x_2, 0) = 0 \quad (0 \le x_1 \le L/2, 0 \le x_2 \le W) \tag{9}$$

$$\sigma_{23}^{\delta}(x_1, x_2, 0) = 0 \quad (0 \le x_1 \le L/2, 0 \le x_2 \le W) \tag{10}$$

$$\sigma_{13}^{\delta}(x_1, x_2, 0) = 0 \quad (0 \le x_1 \le L/2, 0 \le x_2 \le W) \tag{11}$$

$$(\delta = f, m, c)$$

where u_0 is the prescribed displacement in the direction of the loading axis. In addition to the symmetry conditions, one node was fixed in the x_2-direction to prevent rigid body motion.

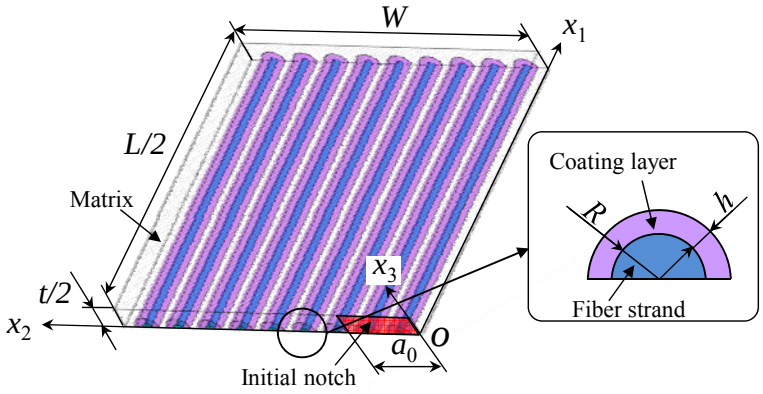

Figure 3 Finite element model of the SENT specimen

Under incrementally applied loading, stress analyses were carried out to identify the damage location according to a failure criterion. The von Mises criterion was selected as the criterion for microcracking of the matrix and the coating layer [5].

$$(\sigma_{22}^{\delta} - \sigma_{33}^{\delta})^2 + (\sigma_{33}^{\delta} - \sigma_{11}^{\delta})^2 + (\sigma_{11}^{\delta} - \sigma_{22}^{\delta})^2 + 6\{(\sigma_{23}^{\delta})^2 + (\sigma_{31}^{\delta})^2 + (\sigma_{12}^{\delta})^2\} \ge 2(\sigma_T^{\delta})^2 \quad (\delta = m, c) \tag{12}$$

where σ_T^{δ} is the tensile strength. The maximum stress criterion was also used to evaluate breaking of the fiber strand.

$$\sigma_{11}^{f} \ge \sigma_T^{f} \tag{13}$$

where σ_T^{f} is the tensile strength of fiber strand. Once the failure criterion is satisfied, all of the stiffness terms are reduced to 1×10^{-4} of the original value.

The epoxy matrix and coating layer are assumed to be elastic and isotropic. For the epoxy matrix, the Young's modulus and Poisson's ratio are taken to be 3.48GPa [6] and 0.35 [7], respectively, and the measured tensile strength is 70MPa. In previous work on this self-healing system [1], an investigation of tensile properties of epoxy specimens with the microcapsule and catalyst revealed that the Young's modulus and tensile strength of the specimen decreased with increasing the microcapsule concentration. Thus, the Young's modulus, Poisson's ratio and tensile strength of the coating layer are assumed to be 1.74GPa, 0.35 and 35MPa, respectively. The carbon fiber strand is modeled as an elastic and transversely isotropic composite (unidirectional carbon/epoxy composite) with properties as shown in Table 1 [8]. (E_1, E_2, E_3) are the Young's moduli, (G_{12}, G_{23}, G_{31}) are the shear moduli and (ν_{12}, ν_{23}, ν_{13}) are the Poisson's ratios, and the Poisson's ratio ν_{12} (ν_{23}, ν_{13})

reflects shrinkage (expansion) in the x_2 (x_3, x_3)-direction due to tensile (compressive) stress in the x_1 (x_2, x_1)-direction.

Table 1 Mechanical properties of the carbon fiber strand

Young's modulus (GPa)		Shear modulus (GPa)		Poisson's ratio		Tensile strength (MPa)
E_1	E_2, E_3	G_{12}, G_{31}	G_{23}	ν_{12}, ν_{13}	ν_{23}	σ_T^f
147	10.3	7.0	3.7	0.27	0.54	2280

3. Results and discussion

Fig. 4 shows typical virgin and damaged load-displacement curves for reference FRP specimens with t=2mm. It was found that the critical fracture load of the damaged specimen (P_c^{damaged}) was almost the same as the value of P_c^{residual}. Typical virgin and healed load-displacement curves for the self-healing FRP specimens with t=2mm are shown in Fig. 5. The slope is initially the same as the virgin test and this indicates that the damage has healed. The healing efficiency for the specimen with t=2mm shown in Fig. 5 is 45%. A healing efficiency of 98% was also achieved for the self-healing FRP specimen with t=3mm, but the healing probability for the specimen with t=3mm was slightly lower than that for the specimen with t=2mm (data not shown).

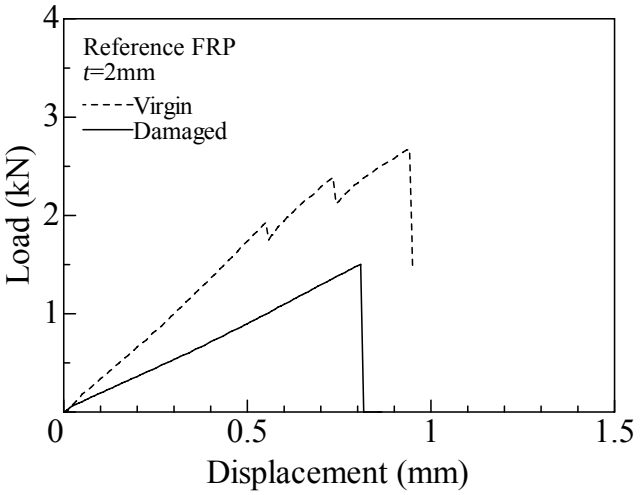

Figure 4 Measured load-displacement curves for reference FRP specimens with t=2mm

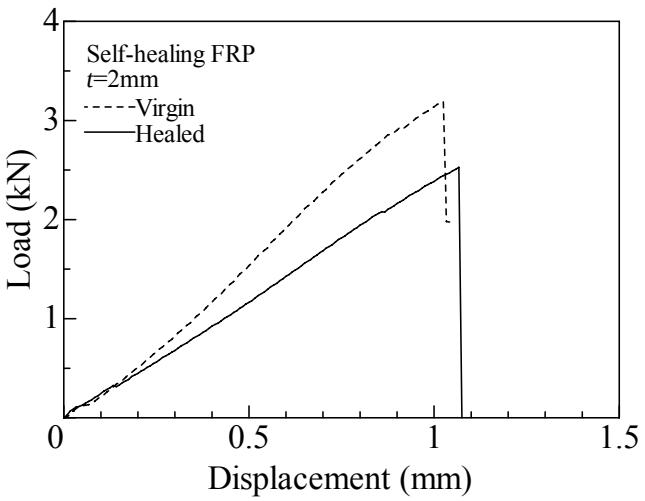

Figure 5 Measured load-displacement curves for self-healing FRP specimens with t=2mm

To investigate the damage progression behavior in the SENT specimen of the self-healing FRP, the finite element analysis coupled with damages was employed. In this analysis, the values of R=0.266mm and h=0.484mm were used. Fig. 6 shows the predicted damage progression in the SENT specimen with t=2mm at the applied displacement value of 0.4mm. The microcracking of the matrix initiated from the initial notch tip and propagated along the coated fiber strand. Moreover, the microcracking of the coating layer was followed by the microcracking of the matrix. This leads to the release of the healing agent from the microcapsules. The microcracking of the coating layer close to the fiber strand/coating layer interface also initiated and propagated, and could induce fiber strand/coating layer debonding. The corresponding result for the SENT specimen with t=3mm at applied displacement value of 0.5mm is shown in Fig. 7. The microcracking of the matrix initiated from the initial notch tip, and the microcracking of coating layer was followed by the

microcracking of the matrix. The microcracking of the matrix then propagated toward the edge of the specimen and induced final failure of the specimen. It is found that the prediction of the initiation and progression of the damage is in good agreement with experimental results.

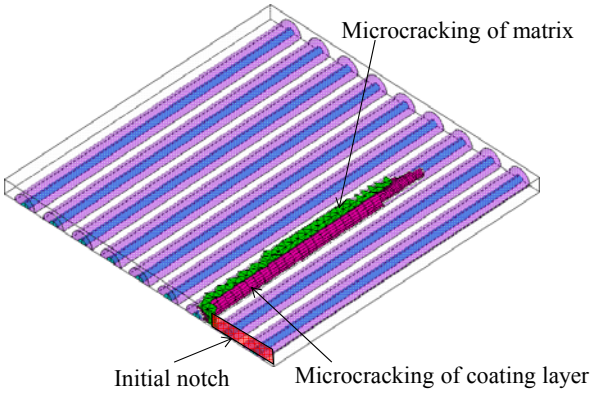

Figure 6 Predicted damage growth pattern in a SENT specimen with t=2mm at the applied displacement value of 0.4mm

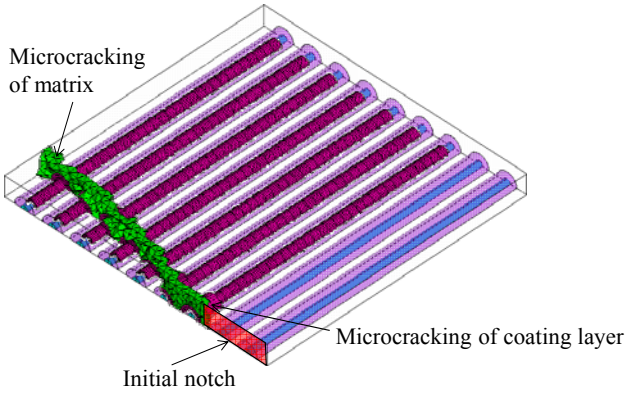

Figure 7 Predicted damage growth pattern in a SENT specimen with t=3mm at the applied displacement value of 0.5mm

In conclusion, we demonstrated that several SENT specimens of self-healing FRP exhibited damage progression along the coated fiber strands and achieved successful healing. Moreover, the numerical and experimental results showed similar trends.

References

[1] K. Sanada, I. Yasuda, Y. Shindo, Transverse tensile strength of unidirectional fibre-reinforced polymers and self-healing of interfacial debonding, Plast Rubber Compos, 35(2006)67-72.

[2] S.R. White, N.R. Sottos, P.H. Geubelle, J.S. Moore, M.R. Kessler, S.R. Sriram, E.N. Brown, S. Viswanathan, Autonomic healing of polymer composites, Nature, 409(2001)794-797.

[3] K. Sanada, N. Itaya, Y. Shindo, Self-healing of interfacial debonding in fiber-reinforced polymers and effect of microstructure on strength recovery, The Open Mech Engng J, 2(2008)97-103.

[4] B.J. Blaiszik, M. Baginska, S.R. White, N.R. Sottos, Autonomic recovery of fiber/matrix interfacial bond strength in a model composite, Adv Funct Mater, 20(2010)3547-3554.

[5] L.G. Zhao, N.A. Warrior, A.C. Long, Finite element modeling of damage progression in non-crimp fabric reinforced composites, Compos Sci Tech, 66(2006)36-50.

[6] K. Sanada, Y. Takada, S. Yamamoto, Y. Shindo, Analytical and experimental characterization of stiffness and damping in carbon nanocoil reinforced polymer composites, J Solid Mech Mater Engng, 2(2008)1517-1527.

[7] F.J.Guild, A.J. Kinloch, Predictive modeling of the mechanical properties of rubber-toughened epoxy, J Mater Sci Lett, 13(1994)629-632.

[8] I.M. Daniel, O. Ishai, Engineering Mechanics of Composite Materials, Oxford University Press, New York, 2006.